Biosensors and Bioelectronics 119 (2018) 215–220

Contents lists available at ScienceDirect

Biosensors and Bioelectronics

journal homepage: www.elsevier.com/locate/bios

Amperometric DNA biosensor for *Mycobacterium tuberculosis* detection using flower-like carbon nanotubes-polyaniline nanohybrid and enzyme-assisted signal amplification strategy

Yuhan Chen[a,b,1], Shuliang Guo[a,1], Min Zhao[c], Pu Zhang[b], Zhuliu Xin[a], Jiang Tao[a], Lijuan Bai[b,*]

[a] Department of Respiratory Disease, The First Affiliated Hospital of Chongqing Medical University, Chongqing 400016, PR China
[b] Engineering Technology Research Center for Pharmacodynamic Evaluation of Chongqing, College of Pharmacy, Chongqing Medical University, Chongqing 400016, PR China
[c] Key Laboratory of Clinical Laboratory Diagnostics (Ministry of Education), College of Laboratory Medicine, Chongqing Medical University, Chongqing 400016, PR China

ARTICLE INFO

Keywords:
Flower-like nanohybrid
Novel redox nanoprobe and nanocarrier
Mycobacterium tuberculosis
Universal DNA biosensor
Tuberculosis diagnosis

ABSTRACT

The authors described a universal amperometric DNA biosensor for rapid and ultrasensitive detection of the specific IS6110 DNA sequence of *Mycobacterium tuberculosis* (MTB). Surprisingly, when tufted carbon nanotubes (CNTs) doped with polyaniline (PAN), a unique flower-like structure with large surface area, abundant active groups and efficient redox activity was obtained. Accordingly, CNTs-PAN nanohybrid was designed both as novel redox nanoprobe and nanocarrier to decorate signal probe, forming tracer label for the generation and amplification of electrochemical signal. In addition, functionalized fullerene (C_{60}) nanoparticles (FC_{60}) were employed as sensor platform to accelerate electron transfer and increase the loading of capture probe (CP). Moreover, enzyme-assisted target recycling amplification including three-way DNA junction could resolve the restriction of target sequences and make this method universal for other analytes. In the presence of target DNA, the assistant probe (AP), together with target DNA, could hybridize with CP and open its hairpin structure to form the Y-shaped junction and recognition sequence for nicking endonuclease. Once the CP was cleaved, the released AP and target DNA could hybridize with another CP to trigger the next cycle of cleavage, resulting in a large number of cleaved CP. After hybridization between cleaved CP and tracer label, a significantly enhanced electrochemical signal of CNTs-PAN could be easily read out. Based on the multiple signal amplification strategy, a wide detection linear range from 1 fM to 10 nM was obtained for target DNA of MTB. More importantly, the universal DNA biosensor also showed high specificity and sensitivity for MTB detection in clinical samples, which may provide a pragmatic tool for MTB testing and hold a great potential for other analytes.

1. Introduction

Although fighting with tuberculosis (TB) has last for many years, the world is still beset by high burden of this disease, which is mainly caused by the infection of *Mycobacterium tuberculosis* (MTB). But unfortunately, the current method for TB diagnosis is facing great challenge and remaining in its infancy. At present, TB diagnosis mainly relies on MTB detection by microscopic examination and bacterial culture of MTB. However, sputum smear microscopy has low positive rate and poor sensitivity. With regard to bacterial culture, the slow growth of MTB usually takes about 4–6 weeks to yield satisfied result, causing delay diagnosis of TB patients (Steingart et al., 2006; Caceres et al., 2013). To convert this adverse situation, recently, people found the genetic sequence of MTB could be an alternative approach for TB diagnosis. Following this finding, nucleic acid testing methods such as polymerase chain reaction (Lee et al., 2014) and oligonucleotide microarray (Thuong et al., 2008) have been used for detecting MTB and become promising tools for TB diagnosis due to their improved detection performance. However, due to the low concentration of bacterial in specimens and some inherent deficits of these methods, there is still no satisfactory result for TB diagnosis.

So far, electrochemical DNA biosensors have received extensive attention in the field of pathogen diagnosis due to its high sensitivity, low cost and easy simplicity of operator (Su et al., 2011; She et al., 2015). Owing to low concentration of pathogenic organisms in organism, nanomaterials and biological amplification technologies are

* Corresponding author.
E-mail address: bailijua88@126.com (L. Bai).
[1] These two authors contributed equally to this work.

https://doi.org/10.1016/j.bios.2018.08.023
Received 8 June 2018; Received in revised form 2 August 2018; Accepted 10 August 2018
Available online 11 August 2018
0956-5663/

widely employed in electrochemical DNA biosensors to enhance detection sensitivity (Chen et al., 2013; Dong et al., 2015). Polyaniline (PAN), with large surface area, high conductivity, environmental stability and unique electrical properties, has been utilized in many fields, including supercapacitors (Meng et al., 2010), batteries (Wu et al., 2013) and biosensors (Ji et al., 2008). Nevertheless, to our best knowledge, only few studies considering the redox property of PAN focus on electrochemical detection (Dhand et al., 2011). Since the redox signal of PAN can only be obtained in strong acid solution, while most bioanalytes cannot stand this unfriendly environment and there is a large impediment in its wide application (Ding et al., 2007). Fortunately, we previously found that carbon material can improve the intrinsic redox activity of PAN (Bai et al., 2017; Chen et al., 2017). When PAN was doped with some certain kinds of carbon nanomaterials, the designed nanohybrids exhibited better redox activity and conductivity performances than that of pure PAN in neutral condition, which provided innovative strategies for the generation and amplification of response signal in electrochemical biosensors to enhance the detection performances.

With regard to other carbon nanomaterials, carbon nanotubes (CNTs) has attracted considerable attention due to its high aspect ratio, outstanding conductivity and strong thermal stability (Guldi et al., 2006; Trojanowicz, 2006). More interestingly, we found that when tufted CNTs doped with PAN, the CNTs-PAN nanohybrid displayed unique flower-like structure and possessed larger surface area than that of sole CNTs and PAN, which would provide extra advantages according to some related literatures. For example, Dong et al. (2018) found that the wool-ball-like structure of La-based MOFs may provide more active sites to increase enzyme immobilization amount and thus have a superior electrochemical sensing performance towards H_2O_2 detection. Wang et al. (2016) reported that a flower-like HKUST-1 showed increasing catalytic ability, which was subsequently used in detection of hydrogen peroxide in biological samples. In this work, flower-like CNTs-PAN nanohybrid not only possessed large surface area with abundant amine groups for further modification, but also displayed excellent electronic conductivity and redox activity, which mainly benefited from the unique synergistic effect of the two components. On the basis of these remarkable advantages, CNTs-PAN nanohybrid was employed both as a novel redox nanoprobe and an ideal nanocarrier in the designed amperometric DNA biosensor.

On the other hand, nucleic acid test based on molecular hybridization is often a 1:1 recognition system between capture probe and signal tag, which may lead to low signal response and can not meet the requirement of highly sensitive detection (Liu et al., 2012). In order to overcome the shortcoming of traditional method and enhance the sensitivity of detection method, enzyme-assisted amplification strategy was developed. For example. Chen et al. (2010) presented a sensitive DNA electrochemical biosensor based on nicking endonuclease assisted strategy. Zuo et al. (2010) introduced a exonuclease III-aided target recycling strategy in fluorescence DNA detection for signal amplification. These methods changed the 1:1 recognition system because the target can be used for many cycles, resulting in enhanced detection sensitivity. However, the major limitation of these methods was the limitation of nucleotide sequence for target DNA, because the specific cleaved site of nuclease was generally located in target DNA, which restricted the wide application of these methods. Recently, a novel enzyme-assisted target recycling amplification strategy has owned great popularity due to its unique enzyme digestion process (Wang et al., 2012). This strategy consists of a three-way DNA junction-aided enzymatic recycling process and the cleavage site of nicking endonuclease is isolated from target, which could overcome the restriction of target DNA sequences. Therefore, it is possible to flexibly change the sequence of capture probe and assistant probe according to different target analytes, greatly expanding its application.

Herein, a new electrochemical DNA biosensor for ultrasensitive detection of the specific IS6110 DNA sequence of MTB was constructed by using CNTs-PAN nanohybrid and enzyme-assisted signal amplification strategy. First of all, electrodeposited gold nanoparticles (AuNPs) combined with functionalized fullerene (C_{60}) nanoparticles (FC_{60}) had large surface area and high conductivity, which provided a suitable sensing platform to facilitate electron transfer and increase the loading of capture probe (CP). Secondly, the flower-like CNTs-PAN nanohybrid with large surface area, excellent redox activity and abundant amine groups could be decorated with AuNPs and labeled with signal probe to form a new tracer label for the generation and amplification of electrochemical signal. In addition, a nicking endonuclease assisted three-way DNA junction system was introduced for target DNA recycling, which could overcome the restriction of target sequence, making this method universal in wide field of bioanalysis. When target DNA was introduced in this system, the assistant probe (AP), together with target DNA, could hybridize with CP and open its hairpin structure to form a Y-shaped junction, as well as form the double-stranded recognition sequence for Nt.BbvCI. Once the CP was cleaved from the junction, the released target DNA combined with AP could hybridize with another CP and initiate the next cycle, resulting in a large number of cleaved CP. After the hybridization between cleaved CP and tracer label, a significantly enhanced electrochemical signal of CNTs-PAN could be easily read out. As a result, the designed DNA biosensor may provide a universal and powerful tool for other pathogenic microorganism and biomolecules in laboratory and clinical application. The stepwise fabrication process of the biosensor, the preparation procedure of tracer label, as well as the Y-shaped junction structure of the proposed sensing system, were depicted and discussed in detail in Fig. 1A, B and C, respectively.

2. Experimental

2.1. Reagents and materials

Cholorauric acid ($HAuCl_4$), poly (diallyldimethylammonium chloride) (PDDA, 30%), poly (amino-amine) dendrimers (PAMAM, 5 wt % in methanol) were purchased from Sigma-Aldrich Chemical Co. (USA). Carbon nanotubes (CNTs) and fullerene (C_{60}, 99.5%) were purchased from XFNANO Nanotechnology Co., Ltd (Nanjing, China). Potassium persulfate ($K_2S_2O_8$, 99%) and bovine serum albumin (BSA) were purchased from J&K Scientific Ltd (Beijing, China). Nicking endonuclease (Nt.BbvCI) and NEB buffer were purchased from New England Biolabs Ltd. (Beijing, China). Patients' sputum samples were supplied by the First Affiliated Hospital of Chongqing Medical University. DNA dissolution and dilution was achieved using 10 mM Tris-HCl buffer (pH 7.4) containing 50 mM KCl and 1 mM $MgCl_2$. Solution of $K_3[Fe(CN)_6]/K_4[Fe(CN)_6]$ (5 mM) containing 0.1 M KCl was used to characterize stepwise fabrication process of the DNA biosensor. Phosphate buffer (0.1 M, pH 7.0) containing 2 mM $MgCl_2$ and 10 mM KCl was used throughout the experiment. All other reagents were of analytical grade. The specific IS6110 DNA sequence was used as target DNA of MTB throughout the experiment. All oligonucleotides were provided by Sangon Biotech. Co. Ltd. and the details of each oligonucleotide sequences were listed in Table S1 (see Supplementary material).

2.2. Apparatus and characterization

Differential pulse voltammetry (DPV), cyclic voltammetry (CV) and electrochemical impedance spectroscopy (EIS) measurements were carried out using a CHI660E electrochemical work station (Shanghai Chenhua Instrument Co, China). The electrochemical detection was taken with a three-electrode system: modified glass carbon electrode (GCE, 4 mm in diameter) as working electrode, platinum wire as auxiliary electrode, saturated calomel electrode (SCE) as reference electrode, respectively. The morphologies of the as-synthesized nanomaterials were characterized by field emission scanning electron

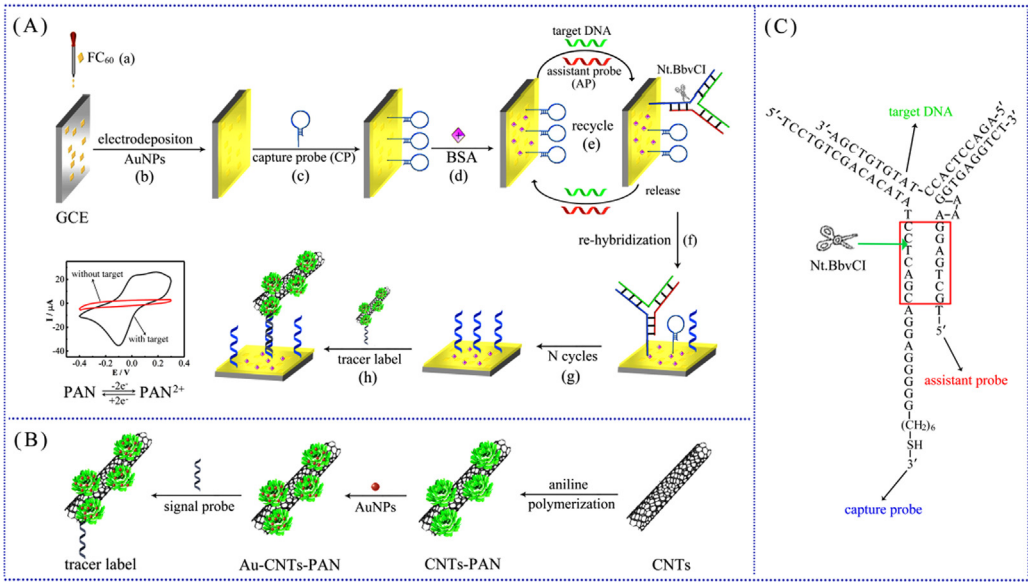

Fig. 1. (A) Schematic representation of the stepwise fabrication process of the electrochemical DNA biosensor: (a) FC_{60} modified GCE; (b) electrodepositing AuNPs on the surface of FC_{60}/GCE; (c) assembling capture probe on AuNPs/FC_{60}/GCE; (d) blocking nonspecific sites with BSA; (e)-(g) target recycling process based on nicking endonuclease-assisted three-way DNA junction process; (h) hybridization between cleaved capture probe and tracer label for electrochemical signal generation. (B) Illustration of the preparation procedure of the tracer label. (C) The Y-shaped three-way DNA junction structure of the proposed sensing system, which contains a two "A" bases unpaired bulge in assistant probe and recognition sequence for Nt.BbvCI (in red box) in assistant probe and capture probe. The arrow marked between two bases in capture probe is the cleavage site.

microscopy (FE-SEM, JSM7800F, Japan) and Transmission electron microscopy (TEM, itachi-7500158, Hitachi Co., Ltd, Japan). X-ray photoelectron spectroscopy (XPS) was carried out using a VG Scientific ESCALAB 250 spectrometer (Thermoelectricity Instruments, USA). Fourier transform infrared spectroscopy (FTIR) was recorded on a Nicolet 6700 FTIR spectrometer (Thermo Nicole, USA). UV–vis absorption was obtained with a U1800 spectrophotometer (Shimazu, Japan). PCR amplification was carried out using MJ MINITM Personal thermal cycler (Bio-Rad, Singapore) and subsequent visualization was obtained with an imaging system (Bio-rad, Italy).

2.3. Fabrication of the electrochemical DNA biosensor

First, functionalized C_{60} nanoparticles (FC_{60}) were prepared according to the literature with a little modification (Han et al., 2015). The details for preparation of FC_{60}, CNTs-PAN and tracer label were shown in Supplementary material. Prior to use, bare GCE was initially polished with 0.3 and 0.05 μm alumina powder respectively, then it was rinsed with water and ethanol for 5 min. Subsequently, 6 μL of FC_{60} solution was placed on the mirror-like surface and dried in the air, followed by electrodeposition of $HAuCl_4$ (1%) to obtain uniformly AuNPs layer. Then 20 μL of capture probe (5 μM) was dripped onto the modified electrode surface and incubated overnight at room temperature. After washing with ultrapure water to remove unbound capture probe, 20 μL of BSA (1%) was placed on the electrode surface for 1 h to block the nonspecific binding site. Next, 20 μL mixture solution containing 10 μL different concentrations of target DNA, 7.5 μL assistant probe (2 μM), 0.5 μL Nt.BbvCI (10,000 U/mL) and 2 μL NEB buffer was placed on the as-pretreated surface of electrode and incubated for 1 h at 37 °C. Last, 10 μL of tracer label solution was added and hybridized at 37 °C for 1.5 h. After that, outstanding electrochemical response signal can be easily read out by DPV measurements (the potential from − 0.4 to 0.3 V with 50 mV pulse amplitude and 50 ms pulse width) in 0.1 M phosphate buffer (pH 7.0). Fig. 1 showed the fabrication process and sensing mechanism of the proposed electrochemical DNA biosensor.

2.4. Analysis of clinical application

Twenty-seven groups of sputum samples (20 groups from TB patients and 7 groups from other patients) were collected from the First Affiliated Hospital of Chongqing Medical University. To ensure the quality of clinical samples, sputum specimens from different patients were collected (more than 1 mL per specimen) early morning and stored at − 80 °C until use. Then each specimen (1 mL) was treated with 5 mL NaOH solution (1 M) at 37 °C for 1 h to obtain liquefied sputum. After centrifugation, the precipitate was resuspended in 1 mL distilled water. Next, genomic DNA was extracted by a TIANamp Bacteria DNA Kit. Afterward, PCR amplification (total 25 μL containing 4 μL genomic DNA) was carried out as follows: initially denatured at 94 °C for 2 min followed by 35 cycles of 94 °C for 30 s, 62 °C for 30 s, 72 °C for 1 min and 1 cycle of 72 °C for 5 min. In order to obtain single-stranded DNA (ssDNA), the PCR production was heated at 100 °C for 7 min and immediately placed on the cold ice for 5 min. The resulting ssDNA was further used for electrochemical analysis.

3. Results and discussion

3.1. Sensing mechanism of the three-way DNA junction

To further explain the sensing mechanism of the three-way junction amplification strategy and evaluate the specific roles of employed assistant probe (AP) and Nt.BbvCI, control experiments were tested. As shown in Fig. 2A, the proposed DNA biosensor (incubated with 10 nM target DNA) exhibited an outstanding current response (curve a). When target DNA or AP was absent in the sensing system, the hairpin of capture probe (CP) can not be opened and it was unable to form the double stranded recognition sequence for Nt.BbvCI. Therefore, there was no cleaved CP to hybridize with tracer label and only negligible background signal responses could be observed (curve b and c). In the absence of Nt.BbvCI, the Y-shaped three-way DNA junction would stably exist on electrode surface, while the tracer label also could not hybridize with CP. As a consequence, no remarkable electrochemical response signal was introduced (curve d).

The gel electrophoresis experiment was further employed to demonstrate the procedure of nicking enzyme-assisted three-way junction amplification strategy. In Fig. 2B, lanes 1–4 showed the electrophoresis images of CP, CP mixed with 10 nM target DNA and Nt.BbvCI, CP mixed with AP and Nt.BbvCI and CP mixed with AP and 10 nM target DNA, respectively. The electrophoresis lanes 2 and 3 showed almost the same location as lane 1, suggesting that only target DNA or AP can not open the hairpin structure of capture DNA. When target DNA and AP were both introduced in absence of Nt.BbvCI (lane 4), some diffuse bands appeared besides the main band, owing to the formation of some Y-shaped junctions. These results were in accordance with that of

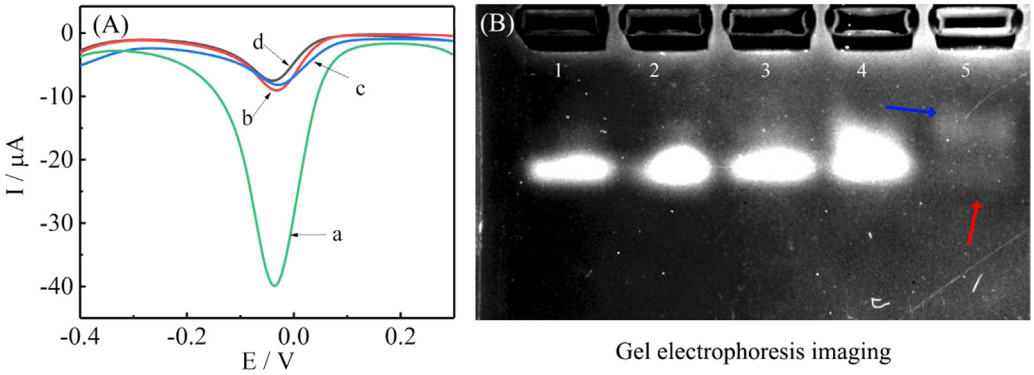

Fig. 2. (A) DVP responses of different modified electrodes: (a) the proposed biosensor incubated with 10 nM target DNA; (b) without assistant probe; (c) without target DNA; (d) without Nt.BbvCI. (B) The gel electrophoresis imaging of different sensing system.

electrochemical detection described above. When Nt.BbvCI was added to trigger the recycling process (lane 5), two new bands appeared. The high band (as shown by the blue arrow) was the initial formation of duplex DNA resulted in slow migration. While the low band (as shown by the red arrow) was the resulting cleaved CP contained a large number of short nucleic acid fragments with faster migration. These results confirmed that recycling cleavage of CP was successfully achieved based on nicking enzyme-assisted three-way junction system.

3.2. Characterizations of nanomaterials

The size and morphology of the as-synthesized nanomaterials were measured by FE-SEM. As shown in Fig. 3A, FC_{60} showed irregular polyhedral structure and distributed homogeneously over the surface. Fig. 3B clearly displayed the filiform tubules of CNTs. Interestingly, it could be seen from Fig. 3C that when CNTs doped with PAN, flower-like nanocluster appeared, exhibiting much larger surface area and porous structure. Fig. 3D showed that shining cluster of AuNPs (as shown by the red arrows) were stably attached on the surface of CNTs-PAN, indicating the successful synthesis of Au-CNTs-PAN nanocomposite. Moreover, the structural features of PAN and CNTs-PAN, as well as the morphological properties of CNTs-PAN and Au-CNTs-PAN, were further characterized using UV–vis and FTIR, TEM and XPS, respectively (Fig. S1 and Fig. S2, see Supplementary material).

3.3. Characterization of the electrochemical DNA biosensor

The interface properties of the surface modified electrodes were monitored by EIS. The Nyquist diagrams of redox couple $[Fe(CN)_6]^{3-/4-}$ at different modified electrodes were displayed in Fig. 4A and the semicircle diameter of EIS was equal to the electron transfer resistance (R_{et}). Bare GCE had a relatively high R_{et} (curve a) compared to AuNPs/

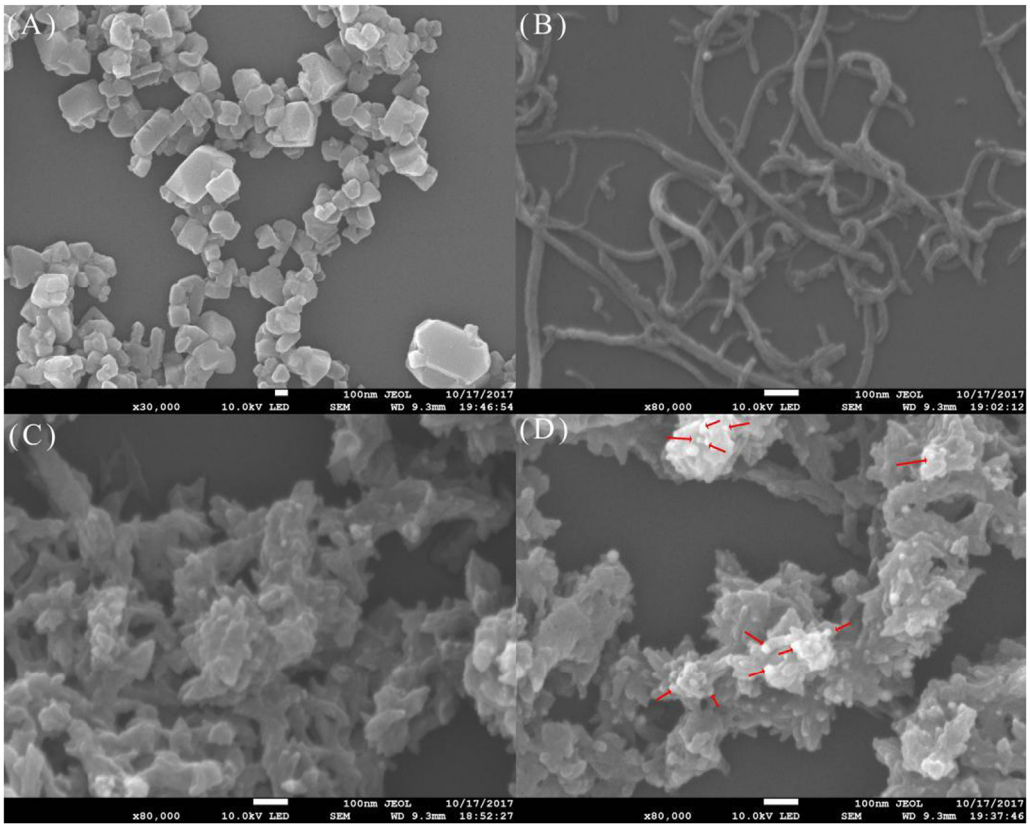

Fig. 3. FE-SEM images of (A) FC_{60}, (B) CNTs, (C) CNTs-PAN and (D) Au-CNTs-PAN.

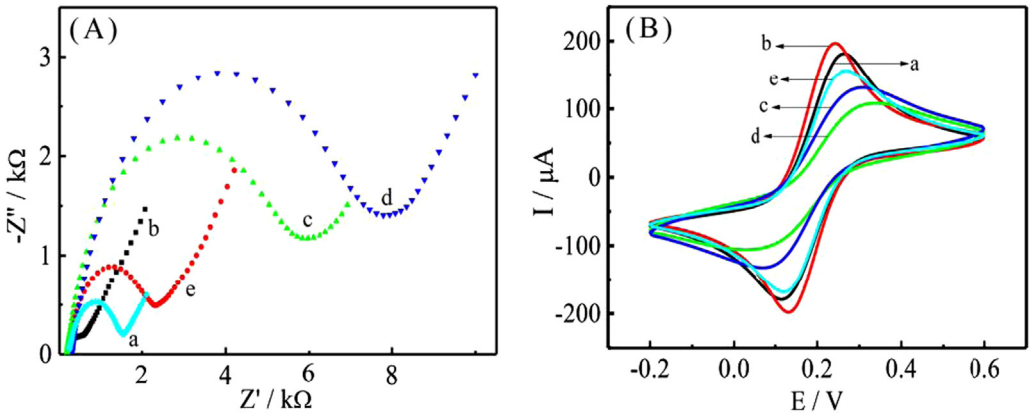

Fig. 4. (A) EIS and (B) CV of different modified electrodes in $K_3[Fe(CN)_6]$/$K_4[Fe(CN)_6]$ solution (5 mM) containing 0.1 M KCl: (a) bare GCE; (b) AuNPs/FC_{60}/GCE; (c) capture probe/AuNPs/FC_{60}/GCE; (d) BSA/capture probe/AuNPs/FC_{60}/GCE; (e) step d incubated with the mixture of assistant probe, target DNA (10 nM) and nicking endonuclease Nt.BbvCI.

FC_{60} modified electrode (curve b), which was attributed to the large surface area and high conductivity of AuNPs and FC_{60}. When capture probe was assembled onto the electrode surface, the stem-loop DNA structure greatly impeded the electron transfer (Xiao et al., 2005), causing the dramatic increase of R_{et} with a big semicircle domain (curve c). After non-conductivity BSA blocked non-specific sites on the electrode surface, further increase of R_{et} was observed (curve d). When the electrode was incubated with the mixture of assistant probe, target DNA and nicking endonuclease, R_{et} decreased greatly (curve e). This may attribute to the formation of Y-junction structure and subsequent cleaved process to produce cleaved capture probe on electrode surface, which reduced the impediment of electron transfer causing by stem-loop capture probe. The stepwise fabrication process of the DNA biosensor was also investigated by CV (Fig. 4B) and the data from CV were in accordance with that from EIS, further indicating the successful construction of the DNA biosensor.

3.4. Analytical performance of the biosensor

To investigate the application of the proposed biosensor for MTB detection, the specific IS6110 DNA sequence of MTB (Marangu et al., 2015) was detected in this experiment and DPV measurements was used to evaluate the performance. As illustrated in Fig. 5A, the peak current increased gradually with the increasing concentrations of target DNA in 0.1 M phosphate buffer (pH 7.0). The standard calibration curve for target DNA detection was shown in Fig. 5B. The peak current was proportional to the logarithm value of target DNA concentration over 7 orders of magnitude range from 1 fM to 10 nM, and the limit of detection (LOD) was estimated as 0.33 fM (S/N = 3). The regression equation was $I = -36.76\ \lg c - 4.364$ with a correlation coefficient of 0.9910.

In addition, the reproducibility of the biosensor was also investigated by using five different electrodes with the same DNA concentration (10 nM). Fig. 5C shows that these electrodes exhibited the closely current response and the relative standard deviation (RSD) was 3.17%, suggesting satisfying reproducibility of our strategy. For the long-term storage stability, as shown in Fig. 5D, the current response of these five electrodes retained from 94.5% to 96.9% of their corresponding initial current response after storage for 10 days (4 °C), which demonstrated that our method presented a good stability. Moreover, the selectivity of the biosensor was studied and the results were shown in Fig. S3 (see Supplementary material), indicating high specificity for target DNA of MTB.

TB diagnostic is often based on direct identification of MTB (Perez-Risco et al., 2018; Yan et al., 2016). LOD was an important factor to analyze the detection performance for MTB testing. For example, Pang et al. (2015) reported a specific real-time PCR, of which the LOD was 250 fold lower compared with conventional real-time PCR, resulting an enhanced sensitivity. Similarly, a multiplexed real-time PCR assay reported with low LOD had achieved a satisfying result compared with the standard method recommend by World Health Organization (Reed et al., 2016). Thus, as shown in Table 1, MTB detection in this work had lower LOD compared with other previous reported methods, which exhibited much higher sensitivity. In addition, this detection method with wider linear range may have the potential to monitor the response of TB treatment in more early stage (Friedrich et al., 2013).

3.5. Clinical sample analysis

Clinical PCR product was often used for assessment of the practical performance of DNA biosensor (Liu et al., 2016; Wang et al., 2014). Thus, twenty-seven groups of clinical PCR products of patients' sputum samples (20 groups from TB patients and 7 groups from other patients) were used to explore the potential application of the proposed DNA biosensor for TB diagnosis. Every sample was repeatedly tested three times for reliable data. The patients' information and results were presented in Fig. S4 and Table S2 (see Supplementary material). The data showed that the 6th, 7th, 16th, 17th, 18th, 22th and 23th groups of sputum samples from non-TB patients exhibited insignificant current response while the rest samples from TB patients showed much higher signal response. The results obtained through electrochemical sensing were in great accordance with that from gel electrophoretic analysis and clinical diagnosis and the RSDs were in range of from 0.5% to 9.4% based on three parallel determination results. Therefore, it was quite evident that the obtained results primitively demonstrate the possibility application of our strategy in clinical practice.

4. Conclusions

In summary, a universal electrochemical DNA biosensor for MTB detection was successfully constructed. Compared with other biosensing for MTB detection, this method showed a superior sensitivity with lower LOD and wider linear range, which attributed to the employment of multiple signal amplification strategy. More importantly, satisfactory results for clinical PCR products determination was obtained, indicating this method may provide a powerful tool for the early diagnosis and monitor of TB disease. It should be noted that the number of clinical samples may not be enough and the clinical samples still need pretreatment of PCR. Therefore, the future work should be done to analysis a large number of clinical specimens to further prove the feasibility and efficiency of our method in clinical application. Meanwhile, it is still important to find the easier way for sample pretreatment, which may further simplify the whole detection process.

Acknowledgements

This work is supported by National Natural Science Foundation of China (81601856), the Third Batch of Young Backbone Teachers

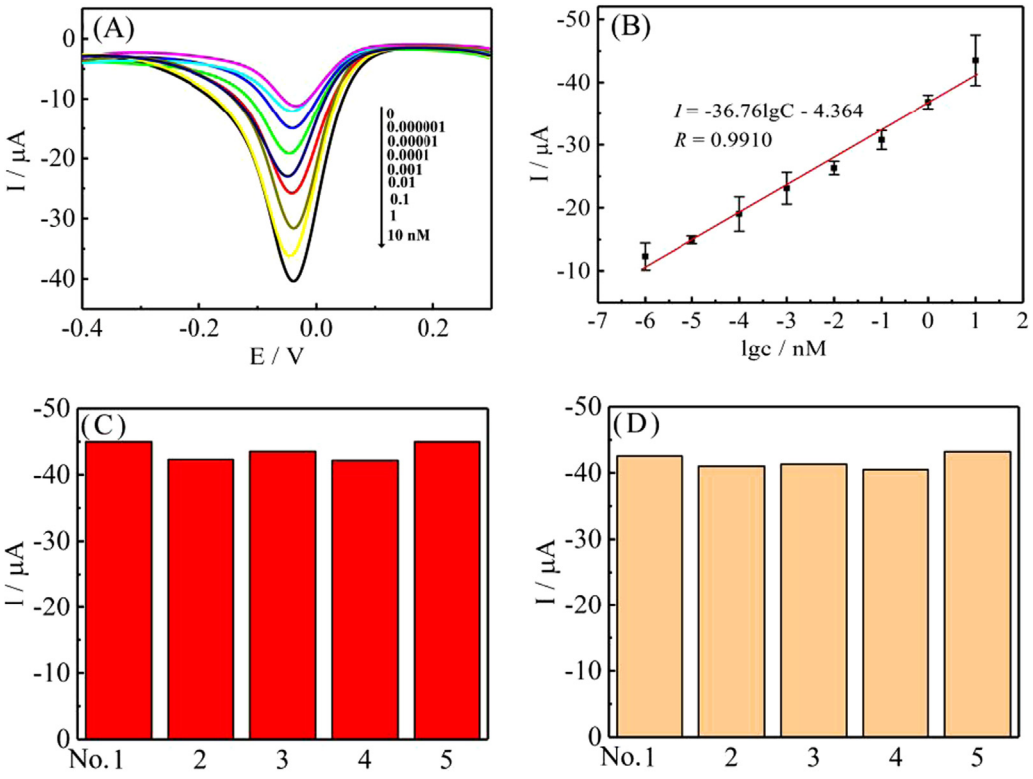

Fig. 5. (A) The peak current obtained by DPV with corresponding concentrations of target DNA (scan range from − 0.4 to 0.3 V, in 0.1 M phosphate buffer). (B) The calibration plots of DPV peak current *versus* the logarithm of target DNA concentration (The error bars represent the standard deviations of three parallel determination results). (C) Reproducibility of the DNA biosensor based on detection of five different electrodes. (D) Long-term stability of the DNA biosensor after 10 days of storage (4 °C) based on the corresponding five electrodes.

Table 1
Detection performances compared with other methodologies for MTB.

Detection method	Linear range	LOD (M)	Ref.
SWV	1.5×10^{-9} –1.25×10^{-8} M	1.3×10^{-9}	(Yesil et al., 2016)
ECL	10^{-10}–10^{-7} M	4×10^{-11}	(Li et al., 2014)
SWV	10^{-14}–10^{-9} M	8.7×10^{-15}	(Zhang et al., 2015)
Impedimetric analysis	10^{-14}–10^{-8} M	10^{-14}	(Perumal et al., 2018)
DPV	10^{-15}–10^{-9} M	3.3×10^{-16}	This work

SWV: square wave voltammetric; ECL: electrochemiluminescence; CV: cyclic voltammetry; DPV: differential pulse voltammetry; LOD: limit of detection.

Funding Program in Colleges and Universities of Chongqing City, China ([2016] No. 53), Funds for Young Science and Technology Talent Cultivation Plan of Chongqing City, China (cstc2014kjrc-qnrc00004) and the National Key Clinical Specialist Construction Programs of China ([2012] No. 649).

Appendix A. Supplementary material

Supplementary data associated with this article can be found in the online version at doi:10.1016/j.bios.2018.08.023

References

Bai, L., Chen, Y., Bai, Y., Chen, Y., Zhou, J., Huang, A., 2017. Biomaterials 133, 11–19.
Caceres, N., Vilaplana, C., Prats, C., Marzo, E., Llopis, I., Valls, J., Lopez, D., Cardona, P.-J., 2013. Tuberculosis 93, 690–698.
Chen, Y., Wang, Q., Xu, J., Xiang, Y., Yuan, R., Chai, Y., 2013. Chem. Commun. 49, 2052–2054.
Chen, Y., Li, Y., Yang, Y., Wu, F., Cao, J., Bai, L., 2017. Microchim. Acta 184, 1801–1808.
Chen, J., Zhang, J., Li, J., Fu, F., Yang, H.H., Chen, G., 2010. Chem. Commun. 46, 5939–5941.
Dhand, C., Das, M., Datta, M., Malhotra, B.D., 2011. Biosens. Bioelectron. 26, 2811–2821.
Ding, H., Wan, M., Wei, Y., 2007. Adv. Mater. 19, 465–469.
Dong, S., Zhao, R., Zhu, J., Lu, X., Li, Y., Qiu, S., Jia, L., Jiao, X., Song, S., Fan, C., Hao, R., Song, H., 2015. ACS Appl. Mater. Interfaces 7, 8834–8842.
Dong, S., Peng, L., Wei, W., Huang, T., 2018. ACS Appl. Mater. Interfaces 10, 14665–14672.
Friedrich, S.O., Rachow, A., Saathoff, E., Singh, K., Mangu, C.D., Dawson, R., Phillips, P.P., Venter, A., Bateson, A., Boehme, C.C., Heinrich, N., Hunt, R.D., Boeree, M.J., Zumla, A., McHugh, T.D., Gillespie, S.H., Diacon, A.H., Hoelscher, M., 2013. Lancet Respir. Med. 1, 462–470.
Guldi, D.M., Rahman, G.M.A., Sgobba, V., Ehli, C., 2006. Chem. Soc. Rev. 35, 471–487.
Han, J., Zhuo, Y., Chai, Y.-Q., Xiang, Y., Yuan, R., 2015. Anal. Chem. 87, 1669–1675.
Ji, S., Li, Y., Yang, M., 2008. Sens. Actuators B: Chem. 133, 644–649.
Lee, S.H., Kim, S.-W., Lee, S., Kim, E., Kim, D.-J., Park, S.P., Lee, E.J., Lee, S.Y., Lee, J.S., Lim, C.S., Kim, W.-K., In, K.H., 2014. Chest 146, 1319–1326.
Liu, A., Wang, K., Weng, S., Lei, Y., Lin, L., Chen, W., Lin, X., Chen, Y., 2012. TrAC Trends Anal. Chem. 37, 101–111.
Li, F., Yu, Y., Li, Q., Zhou, M., Cui, H., 2014. Anal. Chem. 86, 1608–1613.
Liu, L., Xiang, G., Jiang, D., Du, C., Liu, C., Huang, W., Pu, X., 2016. Microchim. Acta 183, 379–387.
Marangu, D., Devine, B., John-Stewart, G., 2015. Int. J. Tuberc. Lung Dis. 19, 1339–1347.
Meng, C., Liu, C., Chen, L., Hu, C., Fan, S., 2010. Nano Lett. 10, 4025–4031.
Pang, Y., Lu, J., Yang, J., Wang, Y., Cohen, C., Ni, X., Zhao, Y., 2015. Tuberculosis 95, 411–414.
Perez-Risco, D., Rodriguez-Temporal, D., Valledor-Sanchez, I., Alcaide, F., 2018. J. Clin. Microbiol.
Perumal, V., Saheed, M.S.M., Mohamed, N.M., Saheed, M.S.M., Murthe, S.S., Gopinath, S.C.B., Chiu, J.-M., 2018. Biosens. Bioelectron. 116, 116–122.
Reed, J.L., Walker, Z.J., Basu, D., Allen, V., Nicol, M.P., Kelso, D.M., McFall, S.M., 2016. Tuberculosis 101, 114–124.
She, Z., Topping, K., Shamsi, M.H., Wang, N., Chan, N.W.C., Kraatz, H.-B., 2015. Anal. Chem. 87, 4218–4224.
Steingart, K.R., Ng, V., Henry, M., Hopewell, P.C., Ramsay, A., Cunningham, J., Urbanczik, R., Perkins, M.D., Aziz, M.A., Pai, M., 2006. Lancet Infect. Dis. 6, 664–674.
Su, J., Zhang, H., Jiang, B., Zheng, H., Chai, Y., Yuan, R., Xiang, Y., 2011. Biosens. Bioelectron. 29, 184–188.
Thuong, N.T., Dunstan, S.J., Chau, T.T., Thorsson, V., Simmons, C.P., Quyen, N.T., Thwaites, G.E., Thi Ngoc Lan, N., Hibberd, M., Teo, Y.Y., Seielstad, M., Aderem, A., Farrar, J.J., Hawn, T.R., 2008. PLoS Pathog. 4, e1000229.
Trojanowicz, M., 2006. TrAC Trends Anal. Chem. 25, 480–489.
Wang, Q., Yang, L., Yang, X., Wang, K., He, L., Zhu, J., Su, T., 2012. Chem. Commun. 48, 2982–2984.
Wang, Q., Yang, Y., Gao, F., Ni, J., Zhang, Y., Lin, Z., 2016. ACS Appl. Mater. Interfaces 8, 32477–32487.
Wang, L., Hua, E., Liang, M., Ma, C., Liu, Z., Sheng, S., Liu, M., Xie, G., Feng, W., 2014. Biosens. Bioelectron. 51, 201–207.
Wu, H., Yu, G., Pan, L., Liu, N., McDowell, M.T., Bao, Z., Cui, Y., 2013. Nat. Commun. 4, 1943.
Xiao, Y., Piorek, B.D., Plaxco, K.W., Heeger, A.J., 2005. J. Am. Chem. Soc. 127, 17990–17991.
Yan, L., Xiao, H., Zhang, Q., 2016. Tuberculosis 96, 75–86.
Yesil, M., Donmez, S., Arslan, F., 2016. J. Chem. Sci. 128, 1823–1829.
Zhang, C., Lou, J., Tu, W., Bao, J., Dai, Z., 2015. Analyst 140, 506–511.
Zuo, X., Xia, F., Xiao, Y., Plaxco, K.W., 2010. J. Am. Chem. Soc. 132, 1816–1818.